JMEPEG (2020) 29:4404–4411
https://doi.org/10.1007/s11665-020-04980-x

1059-9495/$19.00

Microstructures and Mechanical Properties of an Al-Zn-Mg-Cu Alloy Processed by Two-Step Aging Treatment

Feng Wang, Yanli Gong, Yong Du, and Min Song

(Submitted May 5, 2020; in revised form June 24, 2020; published online July 21, 2020)

In this paper, the mechanical properties and microstructures of an Al-Zn-Mg-Cu alloy subject to two-step aging treatment were systematically investigated. The results indicate that the mechanical strength and tensile ductility of the alloy can be significantly improved by pre-aging treatment at 120 °C for 6 h and then by second-step aging treatment at 165 °C for 12 h. After second-step aging treatment at 165 °C for 12 h, the tensile strength and yield strength of the alloy reach 718 and 654 MPa, increased by ~ 23 and ~ 35%, respectively, compared to the alloy without aging treatment. The increment in the strength is mainly attributed to the formation of ultrafine metastable η' phase dispersed in the matrix. The fracture mode of the aging treated alloy includes both intergranular fracture and dimpled transgranular fracture. The coarse grain boundary precipitates ($MgZn_2$ phase) and the wide precipitation free zones are beneficial to the tensile ductility of the alloy.

Keywords Al-Zn-Mg-Cu alloy, mechanical properties, microstructures, two-step aging treatment

1. Introduction

Al-Zn-Mg-Cu alloys are widely used as the indispensable materials in aerospace, transportation and other fields, because of their high specific strength, relatively large ductility, light weight, excellent welding performance and superior corrosion resistance (Ref 1-3). It was found that relatively low contents of Zn and Mg elements are beneficial to the formability and ductility, and an appropriate addition of Cu is beneficial to the yield strength and stress corrosion resistance of the alloys (Ref 4-6). Heat treatments involving solution, quenching and aging treatments are significant processing techniques to improve the comprehensive properties of the Al-Zn-Mg-Cu alloys. The nanosized precipitates formed from supersaturated solid solution play an important role in determining the mechanical properties (Ref 7). That is to say, initial coarse second phase particles are completely or near completely dissolved into the matrix to reach the supersaturated solid solution during solution treatment, and then the supersaturated solid solution is decomposed to form nanosized precipitates dispersed in the matrix during aging process, which is beneficial to preventing dislocation sliding and thus to achieving enhanced strength. By controlling the precipitation process, such as microalloying and aging procedure, the mechanical properties of the alloys can be effectively improved.

Feng Wang, Yong Du, and **Min Song**, State Key Laboratory of Powder Metallurgy, Central South University, Changsha 410083, China; and **Yanli Gong**, Department of Automobile Engineering, Hunan Industry Polytechnic, Changsha 410082, China. Contact e-mail: msong@csu.edu.cn.

During the aging process, a series of metastable precipitates will be formed before the formation of equilibrium phase. The precipitation sequence of the Al-Zn-Mg-Cu alloys is generally accepted as: supersaturated solid solution (SSSS) → GP zones (GP I and GP II) → metastable η' phase ($MgZn_2$) → stable η phase ($MgZn_2$) (Ref 8). GP zones are generally considered to be formed by segregation of solute atoms within a certain temperature range during the early stage of aging, with a spherical morphology and showing a coherent relationship with the matrix (Ref 9). It is universally believed that η' phase is the main strengthening phase of the Al-Zn-Mg-Cu alloys (Ref 10). The η' metastable phase has a hexagonal $MgZn_2$ structure, with the lattice constants of $a = 0.496$ nm and $c = 1.402$ nm, maintaining a semi-coherent relationship with the matrix (Ref 11, 12). With the increase in the aging time, metastable η' phase will be transformed to stable η phase, which also has a hexagonal structure but different lattice parameters to η' phase. Normally the mechanical properties of the alloys will be decreased with the coarseness of the η phase, which is not coherent with the matrix.

In order to further improve the comprehensive properties of the alloys, an effective method is to adjust the aging procedure to controlling the precipitation behavior, since the characteristics of the precipitates affect significantly the mechanical properties of the alloys. Previous investigations showed that the strength of the Al-Zn-Mg-Cu alloys depends mainly on the size and number density of the precipitates (Ref 13), while the fracture toughness depends mainly on coarse intermetallic particles and precipitation free zone (PFZ) along the grain boundaries (Ref 14-16). Normally different heat treatment processes result in significant differences in the microstructures and mechanical properties. The peak-aging treatment can significantly improve the strength, but the two-step over-aging treatment is beneficial to the fracture toughness (Ref 17). In this paper, the microstructure and mechanical properties of an Al-Zn-Mg-Cu alloy processed by two-step aging treatment, with different two-step aging conditions, are studied, and the relationship between the microstructure and mechanical prop-

erties is discussed in order to find a reasonable two-step aging treatment to improve the comprehensive properties of the alloy.

2. Experimental

The alloy used in this study is a commercial 7xxx series aluminum alloy, with the chemical composition of Al-11.68Zn-2.35 Mg-4.28Cu-0.21Zr-0.12Fe (in wt.%). The as-hot-rolled alloy was homogenization annealed at 480 °C for 20 h. The specimens were then solution heat treated at 480 °C for 1 h, followed by immediately water quenching to the room temperature (RT). After that, the specimens were subjected to two-step aging treatment, with the first-step aging being performed at 120 °C for 6 h and the second-step aging being performed at higher temperatures of 155, 165 and 175 °C, respectively, with different heat duration periods from 0 to 24 h.

The evolutions of the micro-Vickers hardness with the aging temperature and aging time were tested by an HVS-5 Vickers hardness tester using 3kgf loading force and 10 s dwell time. Each hardness value was averaged from at least five independent measurements. The tensile tests were carried out on an Instron-3369 mechanical testing machine at room temperature, with a constant loading speed of 1.67×10^{-5} s^{-1}. The microstructure of the alloy and tensile fractography were characterized by an FEI Quanta 250 FEG scanning electron microscope (SEM). The chemical compositions of second phase particles were examined by energy-dispersive x-ray analysis (EDX, MnK resolution at 132 eV). The microstructural features of the specimens under peak-aged condition were characterized by a Titan G2 60-300 transmission electron microscopy (TEM). TEM specimens with a thickness of 100 μm and diameter of 3 mm were prepared by cutting and polishing. These disks were electrolytically polished in an electrolytic solution of 70% methanol and 30% nitric acid at 14 V and − 30 °C. The compositions of the precipitates during aging were determined by EDX analysis.

3. Results and Discussion

3.1 Remnant Phase After Solution and Quenching Treatments

In general, the second phase particles in Al alloys can be divided into three types according to the formation mode: intermetallic compound (constituents) in the original casting structure, dispersed second phase particles (dispersoids) and strengthening precipitates formed during the aging process. Figure 1(a) shows backscatter electron SEM images of the alloy after solution and quenching treatments. It can be seen that the microstructures of the alloy are composed of α_{Al} matrix and white dispersoids mainly distributed in the area adjacent to the grain boundaries. The coarse white dispersoids are the remnant phase that was not dissolved into the matrix during solution treatment, and these particles are detrimental to the mechanical properties of the alloy. According to the EDX-mapping of the white box area in Fig. 1(a) (as shown in Fig. 1b, c, d, and e), all the main elements Al, Zn, Mg and Cu, accompanied by the impurity elements Fe and Si, are uniformly distributed in the α_{Al} matrix of the alloy. However, the elements Mg and Cu were detected to enrich in the white dispersoids, indicating the segregation of Mg and Cu elements in the dispersoids.

EDS analysis was further used to measure the composition of the dispersoids quantitatively. The composition (wt.%) of the second phase particles after solution and quenching treatments was Al (40.15), Cu (40.52), Mg (18.2), Zn (0.84) and Fe (0.18). According to the percentage of their atomic fraction, the chemical composition of the second phase particles is very close to the S (Al_2CuMg) phase, similar to a previous investigation (Ref 18). S phase is generally transformed from eutectic phase during heat treatment and usually occurs along the grain boundaries. Eutectic phase with low melting point can dissolve rapidly during the solution heat treatment, while brittle S phase is normally difficult to dissolve.

3.2 Hardness Evolution

The hardness evolution can effectively reflect the mechanical response of the alloys subject to aging treatment. Figure 2 shows the Vickers hardness evolution of the alloy during the second-step aging treatment, with different aging temperatures of 155, 165 and 175 °C, respectively. It can be seen that the alloy has obvious aging hardening characteristics during the aging process and all the hardness curves can be divided into under-aged stage, peak-aged stage and over-aged stage. That is to say, the hardness of the alloy increases to a peak-aged condition and then decreases with further increasing the aging preservation. In addition, the alloy aging treated at 165 °C for 12 h shows a maximum peak-aged hardness of 211 Hv, compared to the alloy aging treated at 155 and 175 °C.

3.3 Precipitation Behaviors

3.3.1 Precipitation Behavior at 165 °C at Different Aging Stages. In order to study the effect of the second-step aging time on the microstructural evolution of the alloy, the samples at under-aged (4 h), peak-aged (12 h) and over-aged (20 h) conditions during second-step aging treatment at 165 °C were selected for further microstructural characterization. Figure 3 displays bright-field TEM images and corresponding high-resolution TEM (HRTEM) images of the alloy at different aging stages at 165 °C. Generally, in Al-Zn-Mg-Cu alloys, if the incipient electron beam is along the $< 112 >_{Al}$ zone axis, distinct diffraction spots at 1/2 {311} positions correspond to GP II zones and strong diffraction spots at 1/3 and 2/3 of {220} positions correspond to η' phase (Ref 19). It can be seen from Fig. 3(a) and (b) that elliptical precipitates dominate the microstructures inside the grain at the under-aged stage (4 h). Both HRTEM image and corresponding fast Fourier transformation (FFT) pattern show that the precipitates belong to GP II zone and η' phase. Since the stability of GP II zones is relatively poor, they can be used as the core for the nucleation of the η' phase. At the same time, no GP I zones can be detected. Figure 3(c) and (d) displays the microstructure of the alloy after aging to peak-aged stage (12 h) at 165 °C. It is clearly seen that a large number of the η' precipitates are formed and these η' precipitates play a predominant role in the microstructures after the alloy was aged to 12 h. Therefore, metastable η' phase is the main strengthening precipitates at this stage. In addition, the number density of the precipitates is much higher for the peak-aged alloy, compared to the alloy at the under-aged stage. When the alloy was aged to the over-aged

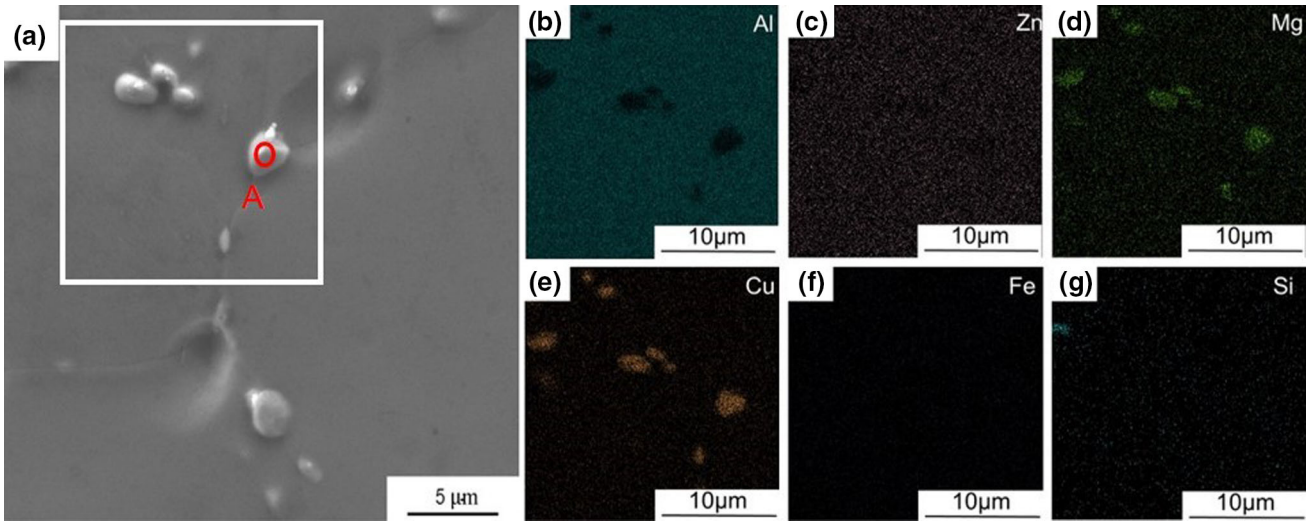

Fig. 1 SEM image and corresponding EDS mapping of the Al-Zn-Mg-Cu alloy after solution and quenching treatments. The composition (wt.%) of the second phase particles after solution and quenching treatments was Al (40.15), Cu (40.52), Mg (18.2), Zn (0.84) and Fe (0.18) by EDS analysis

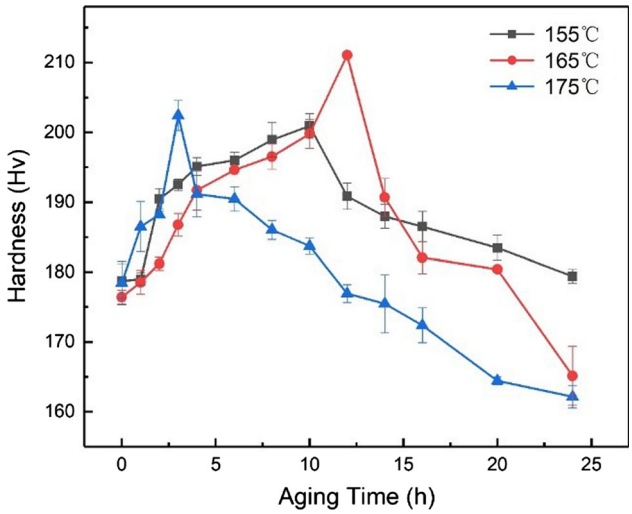

Fig. 2 The hardness curves of the Al-Zn-Mg-Cu alloy during the second-step aging treatment at 155, 165 and 175 °C, respectively

stage (20 h), as shown in Fig. 3(e) and (f), both metastable η' phase and stable η phase can be detected in the microstructures according to the HRTEM image and also the FFT pattern inserted in Fig. 3(f). At the same time, the size of the precipitates increases dramatically, while the number density decreases significantly for the alloy at over-aged stage, compared to the alloy at peak-aged stage.

3.3.2 Precipitation Behaviors at Different Temperatures. Figure 4 shows bright-field TEM images and corresponding HRTEM micrographs viewed along the $< 110 >_{Al}$ zone axis of the peak-aged microstructures of the alloy subject to the second-step aging treatment at 155, 165 and 175 °C, respectively. It can be seen that a large number of elliptical (near sphere) and elongated precipitates are uniformly distributed in the matrix under different aging conditions. Additionally, it can be clearly observed from Fig. 4 that during the second-step aging at 165 °C, the nanoscale precipitates inside the grains are finer than those in the other two conditions and the number density of the precipitates is also much higher. According to the HRTEM images and the FFT patterns from Fig. 4, almost all the precipitates in the alloy subject to peak-aging treatment at different temperatures are semi-coherent platelet η' precipitates and/or elongated η' variants, so the type of precipitates is the same.

The high-angle annular dark-field scanning transmission electron microscope (HAADF-STEM) micrographs of the grain boundaries for the alloy after second-step aging to the peak-aged stage at 155, 165 and 175 °C are presented in Fig. 5, respectively. It can be seen that long rod-shaped precipitates distribute along the grain boundaries in all the conditions. Due to vast defects, plentiful vacancies and high interfacial energy along the grain boundaries, the precipitates evolve much quickly and coarsen significantly. The size of the boundary precipitates is much larger than that of the precipitates inside the grains. Meanwhile, precipitate free zones (PFZs) can be observed in the samples after two-step aging treatment to the peak-aged stages. It can be observed that the width of PFZs increases gradually with the second-step aging temperature. The EDS line scan was performed to measure the chemical composition of the precipitate across the grain boundary, and the results are presented in Fig. 5(d). It can be concluded that the precipitate of grain boundary is the stable η ($MgZn_2$) phase (Ref 20).

3.4 Tensile Properties

3.4.1 Tensile Testing Results. According to the hardness curves, the peak-aged samples at second-step aging process of 155, 165 and 175 °C, accompanied by the samples without aging treatment, are chosen to measure the room temperature tensile properties. The relationship between the true stress and true strain of the samples is shown in Fig. 6. It can be seen that the tensile strength and yield strength of the alloy without aging heat treatment are 584 (± 7) and 485 (± 5) MPa, respectively, while they increase significantly due to the two-step aging treatment. It can be seen that when the second-step aging temperature is 165 °C, the mechanical properties of the alloy

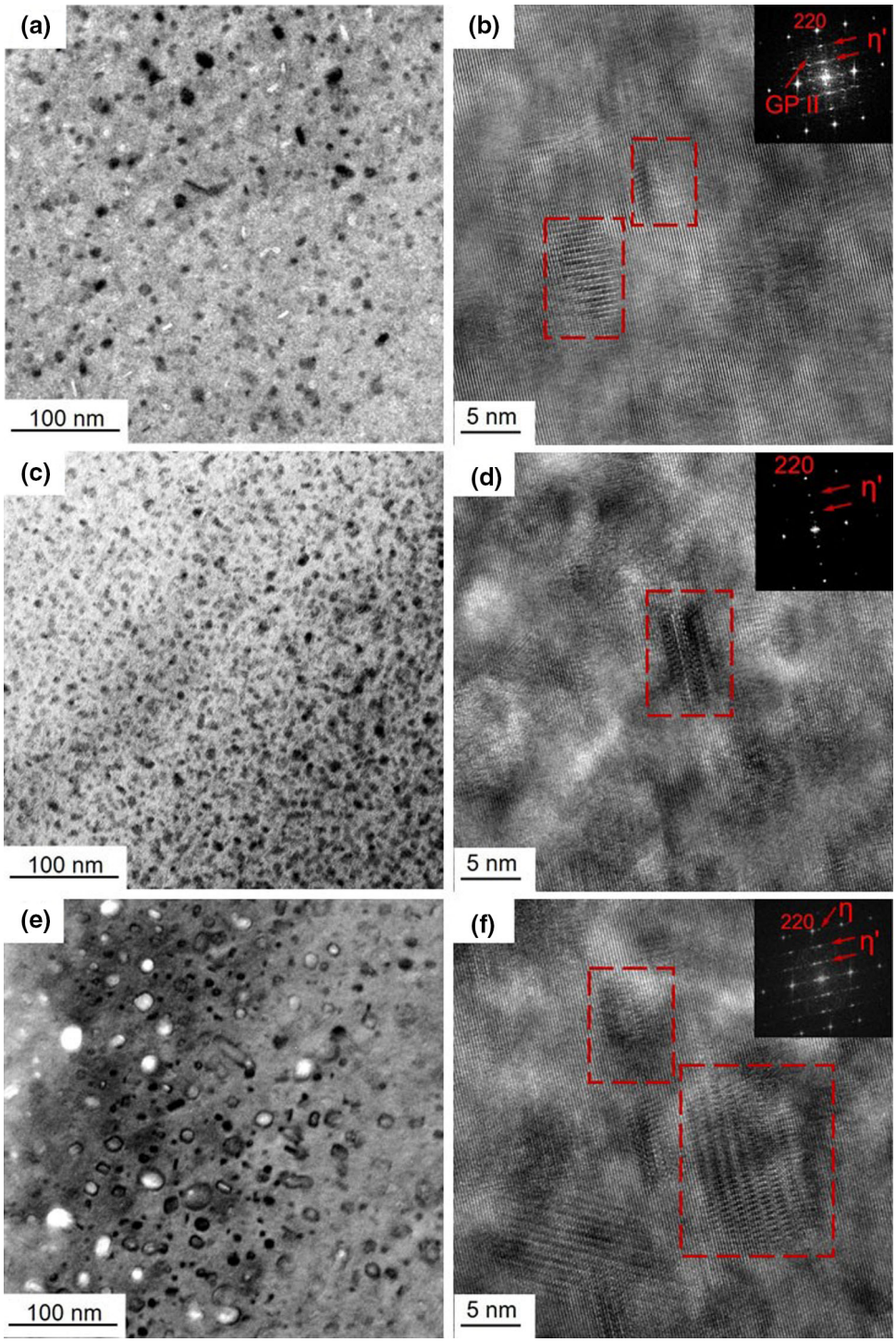

Fig. 3 Bright filed TEM and HRTEM images of the alloy with the electron beam parallel to $<112>_{Al}$ zone axis during the second-step aging treatment at 165 °C for different periods of (a, b) 4 h, (c, d) 12 h and (e, f) 20 h

have the best values, compared to the alloy aging treated at 155 and 175 °C. This result is consistent with the hardness. The tensile strength and yield strength of the alloy after the peak-aging treatment at 165 °C reach 718 (± 11) and 654 (± 6) MPa, with the maximum increment of up to ~ 23 and ~ 35%, respectively. Thus, the two-step aging treatment is very beneficial to improve the strength of the alloy.

For the alloy without heat treatment, there are plenty of coarse second phase particles in the matrix. When the alloy is subject to tensile deformation, the coarse second phase particles are easy to cause stress concentration and this reduce the ductility and strength of the alloy. However, after the alloy was homogenization annealed, the grains were refined due to the addition of Zr. Additionally, a large number of ultrafine nanoprecipitates were formed during the aging treatment, which can hinder the dislocation sliding. Thus, grain refinement and ultrafine nanoprecipitates cause significant increases in both the ductility and strength.

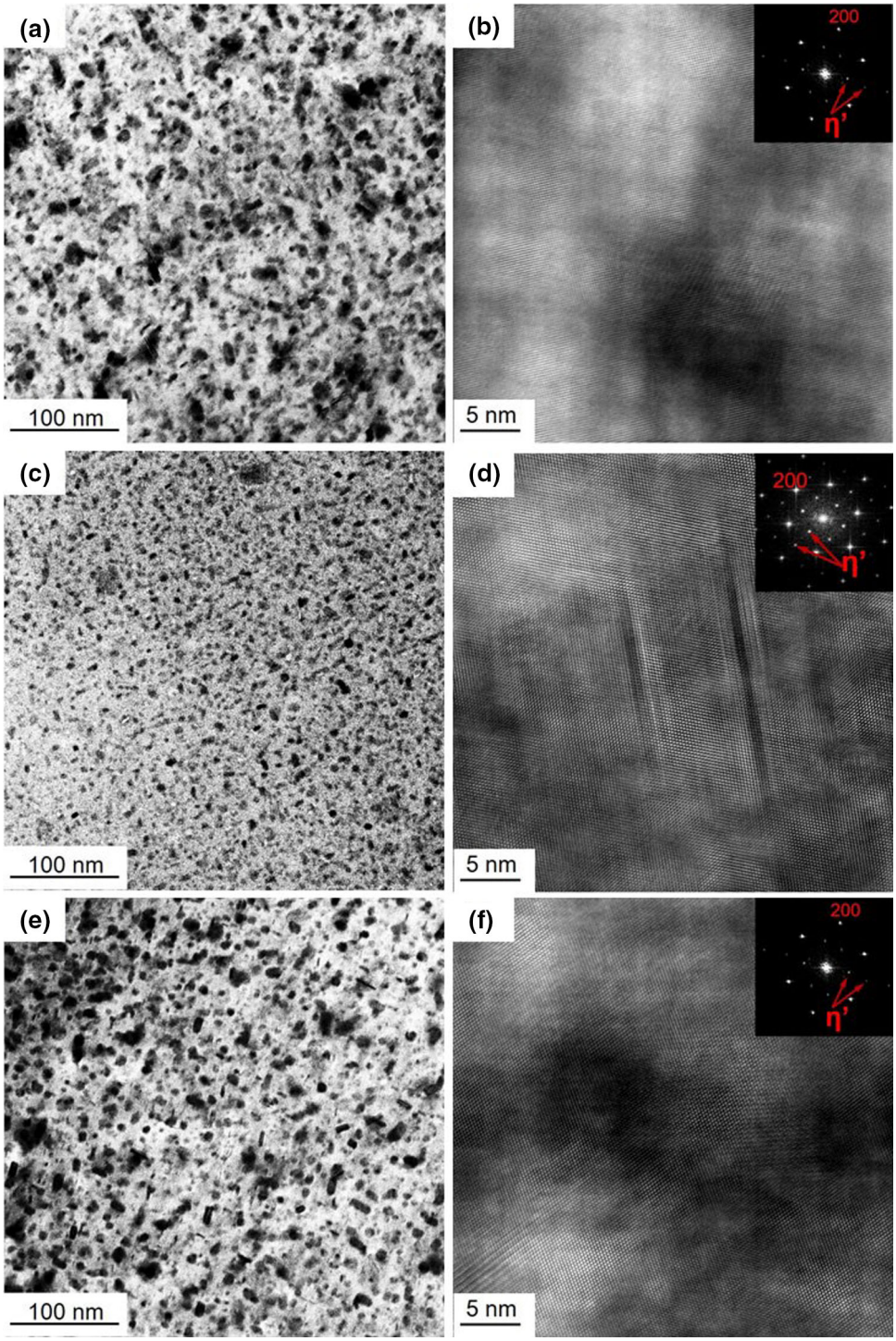

Fig. 4 Bright-field TEM and HRTEM images of the peak-aged alloy with the electron beam parallel to $<110>_{Al}$ zone axis during the second-step aging at (a, b) 155 °C, (c, d) 165 °C and (e, f) 175 °C

3.4.2 Fracture Surfaces. Figure 7 reveals the SEM fracture surfaces of the samples without aging treatment and the samples after the second-step peak-aging treatment at 155, 165 and 175 °C, respectively. As shown in Fig. 7(a), the fracture surface of the alloy without aging treatment is characterized as the intergranular fracture. After two-step aging treatment, the fracture mode of the alloy includes both the intergranular fracture and dimple-induced transgranular fracture, as shown in Fig. 7(b), (c) and (d). Although the dimples of the aging treated samples can be clearly observed, there are differences in the size and the depth of the equiaxial dimples, resulting in the variation in the elongation of the alloy after two-step aging treatment at different temperatures. With the increases in the size and depth of the dimples, the elongation of the alloy can be effectively improved. When the second-stage aging temperature is 175 °C, the size and depth of the dimples increase obviously,

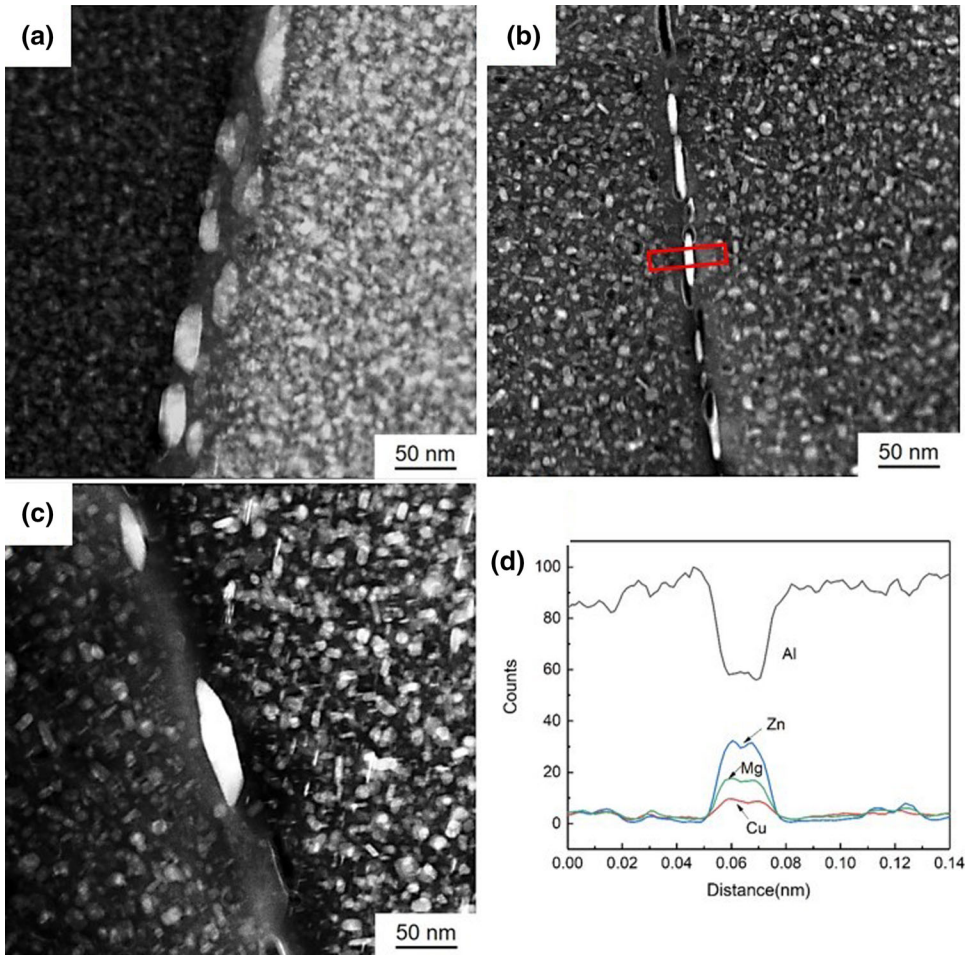

Fig. 5 (a-c) HAADF-STEM micrographs of the grain boundaries of the second-step peak-aged alloy at 155, 165 and 175 °C and (d) EDS line scanning results, showing the element distribution across one precipitate as framed in (b)

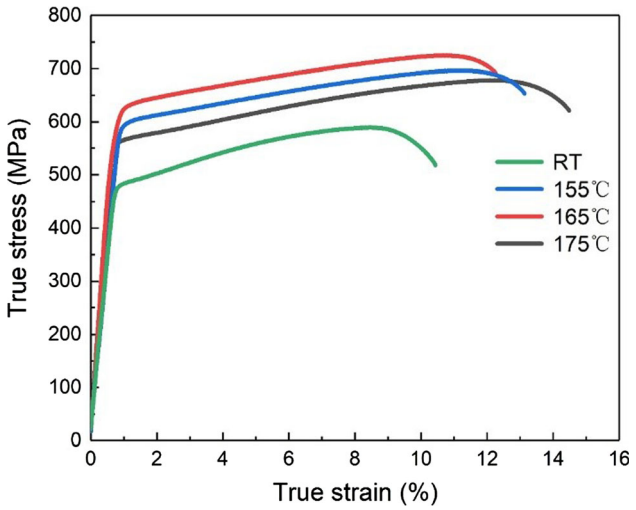

Fig. 6 True stress–true strain curves for the samples after second-step peak-aging treatment at 155, 165 and 175 °C, respectively, and the sample without aging treatment

so the elongation of the alloy is better. At the same time, the existence of second phase particles can be observed inside the dimples. The composition of the second phase inside the dimple was detected by energy-dispersive x-ray (EDX), and the results show that the content of Fe in the particles is substantially higher than that in the matrix, indicating the enrichment of Fe in the particles.

4. Discussion

4.1 The Precipitation Hardening of the Alloy

The existence of the precipitates plays a key role in improving the mechanical properties of the alloy, by hindering the dislocation movements. According to the intrinsic properties of the precipitates, including the hardness, crystalline structure, size, volume fraction and number density, the interaction mode between precipitates and dislocations can be divided into two types: shearing (cutting) and bypassing (Orowan hardening mechanism) (Ref 21). When the precipitates are ultrafine and can be deformed with the matrix, the dislocations can directly cut through the particles, and a new interface will thus be formed between the matrix and precipitates, which in turn leads to the increase in the surface energy and promotes the strengthening effect. This is mainly due to the change of chemical composition or chemical bonding caused by dislocation cutting through the precipitates. The relationship

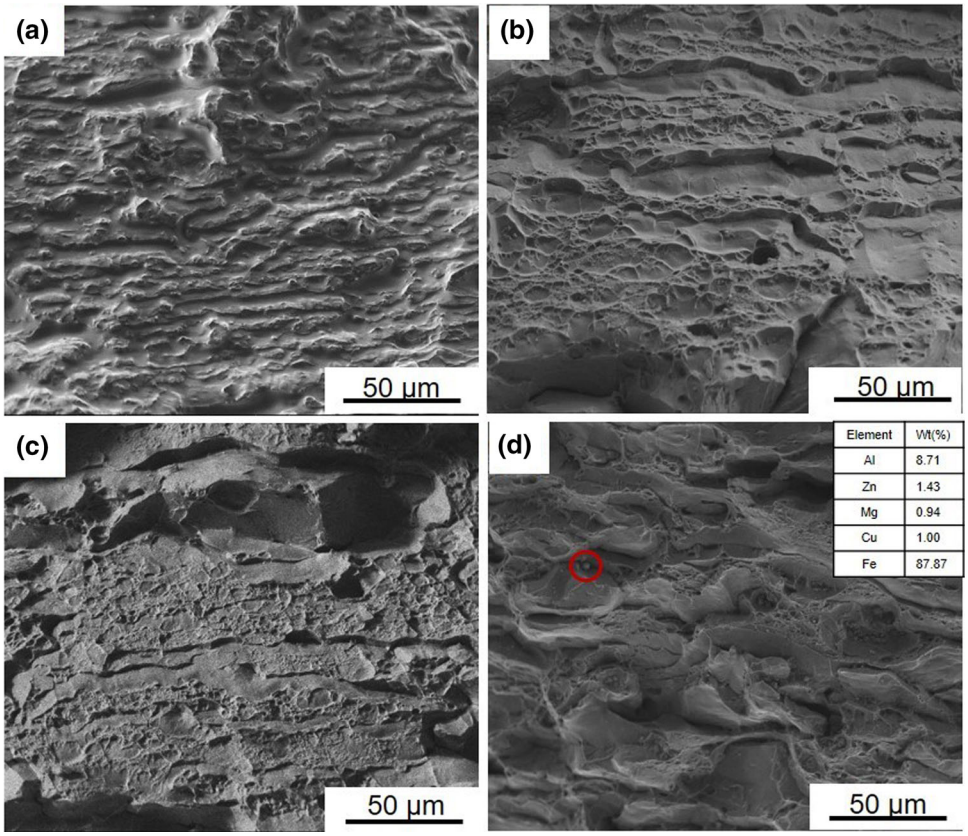

Fig. 7 Fracture surfaces of the tensile fractured Al-Zn-Mg-Cu alloy: (a) without aging treatment, and after second-step peak-aging treatment at (b) 155 °C, (c) 165 °C and (d) 175 °C, respectively

between the resistance $\Delta\tau_1$ caused by dislocation cutting mechanism, the volume fraction f and the radius r of the precipitates can be roughly expressed as: $\Delta\tau_1 \propto f^{1/2}r^{1/2}$ (Ref 22). That is to say, the larger are the precipitates and the higher is the volume fraction, the more significance is the strengthening effect. When the particles are hard (non-deformable or non-shearable), the precipitates are no longer coherent with the matrix and the dislocations act on the precipitates using the bypass mode. The resistance $\Delta\tau_2$ caused by the dislocation bypassing the precipitates can be expressed as $\Delta\tau_2 \propto f^{1/2}r^{-1}$ (Ref 22). So the strength of the alloy decreases with the increase in the precipitate size.

During the second-stage aging process, the precipitates before peak-aged stage are mainly ultrafine semi-coherent η' phase, with a small number of the coherent GP zones, so dislocations mainly cut through the precipitates. With the prolongation of the aging time, the size and volume fraction of the precipitates increase, and the strength of the alloy increases gradually. Simultaneously, the GP zones and η' phase cause lattice distortion, due to the differences between their lattice parameters and elastic modulus, and those of the matrix, which can hinder dislocation movements and thus strengthen the alloy. In the over-aged stage, the precipitates grow up obviously and the interspacing between the precipitates increases. Moreover, stable η phase that is incoherent with the matrix is gradually formed, as shown in Fig. 3(e) and (f). So dislocations mainly bypass the precipitates after peak-aged stage, resulting in the reduction in the strength with precipitates coarsening. In the meantime, incoherent η phase with the matrix reduces the elastic strain energy substantially, and the microstructure of the alloy tends to be stable gradually, also leading to the weakening of the strengthening effect. At different second-step aging temperatures, the strength of the alloy is mainly determined by the size and number density of the precipitates.

4.2 The Fracture of the Alloy

After two-step aging treatment, the elongation of the alloy is closely related to the precipitation free zones (PFZs) and grain boundary precipitates (GBPs). The tensile ductility of the alloy after second-aging at 165 °C is relatively low, compared to the other two aging conditions. It is known that the yield strength of PFZs is significantly lower than that of the matrix strengthened by ultrafine η' phase. When external stress is applied to the alloy, PFZs firstly undergo plastic deformation and crack propagation rate along the grain boundaries is high, leading to intergranular fracture. Then, the plastic deformation enters into the matrix, and the dimple-induced transgranular fracture occurs. On the other hand, during the plastic deformation process, the precipitates distribute continuously along the grain boundary which are prone to deformation incongruity and stress concentration occurs near the grain boundary, resulting in the formation of intergranular fracture.

For the alloy after second-step aging at 175 °C, PFZs are widened and precipitates are coarsened in the matrix, so the difference in yield strength between the matrix and grain boundaries is decreased. Before the cracks on the grain boundary grow up, yielding occurs inside the grains, and then, the cracks inside the grains will grow up rapidly, leading to

transgranular dimple fracture. At the same time, stress relaxation is easy to occur at the PFZs, due to its low strength. As the PFZs widen, stress relaxation increases and cracks are difficult to generate and propagate, which is beneficial to the ductility of the alloy (Ref 23). On the other hand, the large sized η' phase reduces the density of precipitates and increases the space of the dislocation movements, which in turn results in the decrease in the area fraction of the precipitates along the grain boundary. In this way, dislocation is easy to slip and the rate of crack propagation will be reduced. During this aging state, with the interspacing increasing due to the coarsening of η precipitates along the grain boundary, the chance of contact between the cracks and the precipitates on the grain boundary is reduced. So the transgranular fracture caused by the dimples dominates the fracture of 175 °C second-step aging treated alloy (as shown in Fig. 7d), and the tensile ductility of the alloy is increased.

5. Conclusions

In summary, the effects of two-step aging treatment at different temperatures on the mechanical properties and microstructures of an Al-Zn-Mg-Cu alloy were systematically investigated. The two-step aging treatment consists of a pre-aging at 120 °C for 6 h and then a second-step aging at different temperatures for various periods. Second-step aging at 165 °C for 12 h was confirmed to obtain excellent mechanical properties of the alloy. The strengthening effect of peak-aged alloy mainly depends on the homogeneous distributed and ultrafine metastable η' phase inside the grains. After aging treatment, the fracture behaviors of the alloy include both intergranular fracture and dimpled transgranular fracture, leading to the increase in the tensile ductility. In addition, the stable η phase ($MgZn_2$ phase) distributes along the grain boundary discontinuously. The coarse grain boundary precipitates and the wide PFZs are beneficial to the tensile ductility of the alloy.

Acknowledgments

The work is supported by National Natural Science Foundation of China (51531009 and 51820105001). We would like to thank the Advanced Research Center of Central South University for TEM technical support.

References

1. A. Azarniya, A.K. Taheri, and K.K. Taheri, Recent Advances in Ageing of 7xxx Series Aluminum Alloys: A Physical Metallurgy Perspective, *J. Alloy. Compd.*, 2019, **781**, p 945–983
2. T. Dursun and C. Soutis, Recent Developments in Advanced Aircraft Aluminium Alloys, *Mater. Des.*, 2014, **56**, p 862–871
3. E.M. Mazzer, C.R.M. Afonso, M. Galano, C.S. Kiminami, and C. Bolfarini, Microstructure Evolution and Mechanical Properties of Al-Zn-Mg-Cu Alloy Reprocessed by Spray-Forming and Heat Treated at Peak Aged Condition, *J. Alloy. Compd.*, 2013, **579**, p 169–173
4. Y.G. Liao, X.Q. Han, M.X. Zeng, and M. Jin, Influence of Cu on Microstructure and Tensile Properties of 7xxx Series Aluminum Alloy, *Mater. Des.*, 2015, **66**, p 581–586
5. M.X. Guo, J.Q. Du, C.H. Zheng, J.S. Zhang, and L.G. Zhuang, Influence of Zn Contents on Precipitation and Corrosion of Al-Mg-Si-Cu-Zn Alloys for Automotive Applications, *J. Alloy. Compd.*, 2019, **778**, p 256–570
6. P. Xie, S. Chen, K. Chen, H. Jiao, L. Huang, Z. Zhang, and Z. Yang, Enhancing the Stress Corrosion Cracking Resistance of a Low-Cu Containing Al-Zn-Mg-Cu Aluminum Alloy by Step-Quench and Aging Heat Treatment, *Corros. Sci.*, 2019, **161**, p 108184
7. Z. Bai, F. Qiu, Y. Liu, W. Zhou, and Q. Jiang, Age Hardening and Mechanical Properties of Cast Al-Cu Alloy Modified by La and Pr, *Adv. Eng. Mater.*, 2015, **17**, p 143–147
8. G. Sha and A. Cerezo, Early-Stage Precipitation in Al-Zn-Mg-Cu Alloy (7050), *Acta Mater.*, 2004, **52**, p 4503–4516
9. L.K. Berg, J. Gjonnes, V. Hansen, X.Z. Li, M. Knutson-Wedel, G. Waterloo, D. Schryvers, and L.R. Wallenberg, GP-Zones in Al-Zn-Mg Alloys and Their Role in Artificial Aging, *Acta Mater.*, 2001, **49**, p 3443–3451
10. J. Chen, L. Zhen, S. Yang, W. Shao, and S. Dai, Investigation of Precipitation Behavior and Related Hardening in AA 7055 Aluminum Alloy, *Mater. Sci. Eng., A*, 2009, **500**, p 34–42
11. X.Z. Li, V. Hansen, J. Gjonnes, and L.R. Wallenberg, HREM Study and Structure Modeling of the η′ Phase, the Hardening Precipitates in Commercial Al-Zn-Mg Alloys, *Acta Mater.*, 1999, **47**, p 2651–2659
12. C. Wolverton, Crystal Structure and Stability of Complex Precipitate Phases in Al-Cu-Mg-(Si) and Al-Zn-Mg Alloys, *Acta Mater.*, 2001, **49**, p 3129–3142
13. D.M. Liu, B.Q. Xiong, F.G. Bian, Z.H. Li, X.W. Li, Y.G. Zhang, F. Wang, and H.V. Liu, Quantitative Study of Precipitates in an Al-Zn-Mg-Cu Alloy Aged with Various Typical Tempers, *Mater. Sci. Eng., A*, 2013, **588**, p 1–6
14. Z. Cvijović, M. Vratnica, and M. Rakin, Micromechanical Modelling of Fracture Toughness in Overaged 7000 Alloy Forgings, *Mater. Sci. Eng., A*, 2006, **434**, p 339–346
15. Z. Cvijović, M. Rakin, M. Vratnica, and I. Cvijović, Microstructural Dependence of Fracture Toughness in High-Strength 7000 Forging Alloys, *Eng. Fract. Mech.*, 2008, **75**, p 2115–2129
16. O.E. Alarcon, A.M.M. Nazar, and W.A. Monteiro, The Effect of Microstructure on the Mechanical Behavior and Fracture Mechanism in a 7050-T76 Aluminum Alloy, *Mater. Sci. Eng., A*, 1991, **138**, p 275–285
17. N.M. Han, X.M. Zhang, S.D. Liu, B. Ke, and X. Xin, Effects of Pre-stretching and Ageing on the Strength and Fracture Toughness of Aluminum Alloy 7050, *Mater. Sci. Eng., A*, 2011, **528**, p 3714–3721
18. C. Mondal and A.K. Mukhopadhyay, On the Nature of T($Al_2Mg_3Zn_3$) and S(Al_2CuMg) Phases Present in As-Cast and Annealed 7055 Aluminum Alloy, *Mater. Sci. Eng., A*, 2005, **391**, p 367–376
19. K. Wen, B.Q. Xiong, Y.G. Zhang, Z.H. Li, X.W. Li, S.H. Huang, L.Z. Yan, H.W. Yan, and H.W. Liu, Over-Aging Influenced Matrix Precipitate Characteristics Improve Fatigue Crack Propagation in a High Zn-Containing Al-Zn-Mg-Cu Alloy, *Mater. Sci. Eng., A*, 2018, **716**, p 42–54
20. R. Ferragut, A. Somoze, and A. Tolley, Microstructural Evolution of 7012 Alloy during the Early Stages of Artificial Ageing, *Acta Mater.*, 1999, **47**, p 4355–4364
21. J.D. Embury, D.J. Lloyd, and T.R. Ramachandran, 22-Strengthening Mechanisms in Aluminum Alloys, *Treatise Mater. Sci. Technol.*, 1989, **31**, p 579–601
22. H.R. Shercliff and M.F. Ashby, A Process Model for Age Hardening of Aluminium Alloys-I. The Model, *Acta Metall. Mater.*, 1990, **38**, p 1789–1802
23. N. Ryum, The Influence of a Precipitate-Free Zone on the Mechanical Properties of an Al-Mg-Zn Alloy, *Acta Metall.*, 1968, **16**, p 327–332